Frequency-Chirprate Reassignment

Xiangxiang Zhu[a], Haizhao Yang[b], Zhuosheng Zhang[a], Jinghuai Gao[c], Naihao Liu[c]

[a]*School of Mathematics and Statistics, Xi'an Jiaotong University, Xi'an 710049, China*
[b]*Department of Mathematics, Purdue University, West Lafayette, IN, USA, 47907*
[c]*National Engineering Laboratory for Offshore Oil Exploration, Xi'an 710049, China*

Abstract

In this paper, we consider three-dimensional parameter space, which is the time-frequency-chirprate (TFCR), to characterize the time-varying features of multi-component non-stationary signals. By performing reassignment on the frequency-chirprate plane, a highly concentrated TFCR representation, named as the frequency-chirprate reassignment method (FCRM), is proposed. FCRM can provide the instantaneous frequency (IF) and chirprate (CR) estimates jointly, making the time-frequency (TF) crossed signals appear as separated in the TFCR domain, which overcomes the separable limitation of the popular TF post-processing methods. Based on the chirplet transform, we derive the reassignment center of FCRM, and a three-dimension ridge detection algorithm is introduced to extract the IFs and CRs from the FCRM. Numerical experiments demonstrate that FCRM provides a concentrated TFCR representation, obtaining a good IF estimation for overlapped multicomponent signals.

Keywords: Time-frequency-chirprate analysis, Reassignment, Chirplet transform, IF estimation, Overlapped multi-component signals

1. Introduction

Non-stationary signal analysis has received extensive attention in the fields of seismic [1], astronomical [2], radar and sonar [3], biomedicine [4,5], mechanical engineering [6,7], etc. To better process such signals, time-frequency (TF) representations [1,6-8], instead of the Fourier transform, are widely used. The most two popular TF methods are probably the short-time Fourier transform (STFT) [9] and the continuous wavelet transform (CWT) [10], which serve as basic choices for signal detection. However, both transforms are limited by the Heisenberg uncertainty principle [8]. Indeed, the TF resolution is constrained by the choice of window or wavelet, limiting the readability and the adaptivity of the TF representation.

In the past decades, many works have been presented aiming at the high-resolution TF representation, i.e., a sufficient concentration TF plot to represent the signal as accurately as possible. The first attempt we think is the Wigner-Ville distribution (WVD) [11]. Although WVD is not constrained by the uncertainty principle, interference terms are introduced for multi-component signals [8]. Another attempt, called the reassignment method (RM) [12,13], transfers the TF coefficients from the original

Email address: zhuxiagxiang@stu.xjtu.edu.cn (Xiangxiang Zhu)

position to the center of gravity of signal's energy distribution in the TF plane. Although RM improves the energy concentration and has been widely applied in many practical applications [14-16], it lacks an explicit formula for signal reconstruction and fails to characterize signals with cross-over frequencies [17,18].

As a special case of the RM, the synchrosqueezing transform (SST), put forward by Daubechies and Maes in the mid-1990s [19], squeezes the TF coefficients into the IF trajectory only in frequency direction [20]. As a result, SST not only exhibits a TF spectrum with a good readability but also retains an explicit formula for signal reconstruction. In recent years, SST has attracted a lot of interest and been widely studied. It has been proved that SST is adapted to different transform frameworks, including the STFT-based SST [21], the synchrosqueezed curvelet transform [22], the synchrosqueezed wave packet transform [23,24], the synchrosqueezing S-transform [25], the chirplet-based SST [26], etc. The robust analysis and multivariate extensions of SST are presented in [27-31]. In spite of all these advances, one drawback associated with SST in its original formulation is that it suffers from a low TF resolution when dealing with strongly amplitude-modulated and frequency-modulated (AM-FM) signals [32-34], which are very common in many fields of practical interest, e.g., mechanical vibration [7] and gravitational waves [35]. In this regard, many improvements of SST to better handle strong modulation signals are introduced, e.g., the demodulated SST [32,36], the high-order SST [33,37], the multiple squeezes transform [26,38], the time-reassigned SST [39].

Differing from the squeezing manner of SST, the synchroextracting transform (SET) [40] retains only the TF information related to the IFs of the signal and removes most smeared TF energy. A theoretical studies of SET and its extension are presented in [41], which sharpens the TF representation by extracting the TF points satisfying an IF equation. In addition, similar to the time-reassigned SST [39], a time-synchroextracting transform is also developed for transient signals analysis [42].

The introduced TF post-processing methods above, including RM, SST-based methods, and SET-based methods, have been widely used and adapted in many fields [7,14,19,25,27,30,36,37,40,42]. However, the performance of these methods depends on the basic condition of separability, failing in the presence of crossed modes in the TF plane. To tackle this limitation, some attempts have been presented recently. The first one focuses on the modifications of RM [18,43,44] combining with the improved ridge detection methods [45,46]. The modified RM methods correct the signal representation in the non-separable region partly, but no additional support can be used for distinguishing multi-component signal. In addition to the modified RM methods, another two-dimension analysis is referred to as time-chirprate (time-CR) representation, which mainly involves high-order ambiguity functions [47] and cubic phase functions [48,49]. For such methods, cross-terms are also introduced when multi-component signals are considered; however, there is no sufficient study on sharpening the time-CR representation and how to solve the overlapped case in the time-CR plot. Instead of two-dimension signal representation, three-dimension representation (e.g. time-frequency-chirprate (TFCR)) [50,51] shows great potential in processing multi-

component non-stationary signals, since the intersected signals in the TF or time-CR domain frequently appear as separated in high-dimensional space. However, how to obtain an accurate and concentrated three-dimensional representation is a challenging job.

In this paper, we attempt to improve the resolution of the TFCR representation generated by the chirplet transform [41,50,52]. A new transform, named frequency-chirprate reassignment method (FCRM), is proposed, which sharpens the three-dimensional signal representation and characterizes the IF and CR information simultaneously. The main contributions of this paper can be summarized as follows:

(a) We derive the reassignment center for the TFCR representation.

(b) We propose a novel FCRM to obtain a high-resolution TFCR representation by reassigning the frequency-chirprate (frequency-CR) points from original location to reassignment center, which extends the reassignment technology to three-dimensional signal representation.

(c) A three-dimensional ridge detection algorithm is presented to realize the robust detection for IF and CR of the signal.

(d) The FCRM breaks the limitation of the separability of the standard RM and SST methods and has a good performance for handling overlapped multi-component signals.

The remainder of the paper is organized as follows. In Section 2, the TFCR transform is introduced. In Section 3, we devote to the description of the proposed FCRM method. Three-dimensional ridge detection algorithm is given in Section 4. Experimental results and comparative studies are presented in Section 5. Finally, Section 6 concludes the paper.

2. Time-frequency-chirprate representation for multi-component non-stationary signal

2.1. Multi-component non-stationary signal

The multi-component non-stationary signal we considered in this paper is the AM-FM waves as

$$f(t) = \sum_{k=1}^{K} f_k(t) = \sum_{k=1}^{K} A_k(t) e^{j\phi_k(t)}, \tag{1}$$

where K is a positive integer representing the number of AM-FM components, $\sqrt{-1} = j$, $A_k(t) > 0$ and $\phi_k(t)$ are the instantaneous amplitude and instantaneous phase of the k-th component (or mode), respectively. The first and the second derivative of the phase, i.e., $\phi'_k(t)$, $\phi''_k(t)$, are respectively referred to as the instantaneous frequency (IF) and chirprate (CR) of the signal.

Generally, the IFs and CRs of the signal can be used for multi-component and non-stationary signal characterization. Indeed, for $l \neq k$, $(\phi'_l(t), \phi''_l(t)) = (\phi'_k(t), \phi''_k(t))$ requires that these two components to be tangent in the TF plot, which is a more strict condition compared with the intersection in the TF or time-CR plane. That also means the multi-component signal can be well represented by several

separable curves in the TFCR domain for most of the time. Effective signal representation should admit concentrated energy distributions in the IF and CR simultaneously such that post-processing can be carried out for signal estimation and separation.

2.2. Chirplet transform

The chirplet transform (CT) generalizes the STFT by using an extra CR parameter, which is defined as [41,50,52]

$$C_f^g(t,\omega,\beta) = \int_{-\infty}^{+\infty} f(\mu) g(\mu - t) e^{-\frac{j\beta(\mu-t)^2}{2}} e^{-j\omega(\mu-t)} d\mu, \tag{2}$$

where β is the CR parameter/variable, and $g(t)$ is a real and even window function. When $\beta \equiv 0$, this transform corresponds to the well known STFT. By introducing the parameter β, CT maps the signal from the time domain to a three-dimensional space obtaining the TFCR representation.

CT is a linear transform and hence its resolution is limited by the choice of its window size, which is the size of the essential support of g in (2). Indeed, a narrow window leads to a high time-resolution, but diffuses the energy distribution in the frequency-CR domain. Conversely, a wide window produces a concentrated frequency-CR representation, but it causes a large error of the IF estimation for fast-varying signals [36,53,54]. Let us consider an example:

$$\begin{aligned} f(t) &= f_1(t) + f_2(t) + n(t), \\ f_1(t) &= \exp(-0.03t)\sin(2\pi(-90t^2 + 220t)), \\ f_2(t) &= (1 + 0.1\cos(20\pi t))\cos(2\pi(10\sin(2\pi t) + 80t)), \end{aligned} \tag{3}$$

where $n(t)$ is a Gaussian noise. The sampling frequency is 512 Hz, and time duration is [0 1]. The STFT of this test signal with the SNR = 16 dB is illustrated in Fig. 1(a). Fig. 1 (b-c) display the CT slices ($t = 0.5$ s) of this signal using different window lengths, where the red notes are the true instantaneous features of the signal. Obviously, a wide window concentrates the result of $f_1(t)$ but leads the energy distribution of $f_2(t)$ to deviating from the true value. A narrow window is prefer for $f_2(t)$, but it spreads the representation.

3. Frequency-chirprate reassignment method

In this section, we consider how to sharpen the chirplet transform such that the obtained representation concentrates along the IF and CR curves in the TFCR domain. For the convenience of the following explanation, we consider the case of a monocomponent signal $f(t) = A(t)\exp(j\phi(t))$. The multicomponent signals can be handled similarly if all of modes are well separated in the TFCR domain.

Assume that around $\mu = t$ the mode $f(t) = A(t)e^{j\phi(t)}$ can be well approximated by its second-order local expansion:

$$f(\mu + t) \approx A(t) e^{j(\phi(t) + \phi'(t)\mu + \frac{1}{2}\phi''(t)\mu^2)}. \tag{4}$$

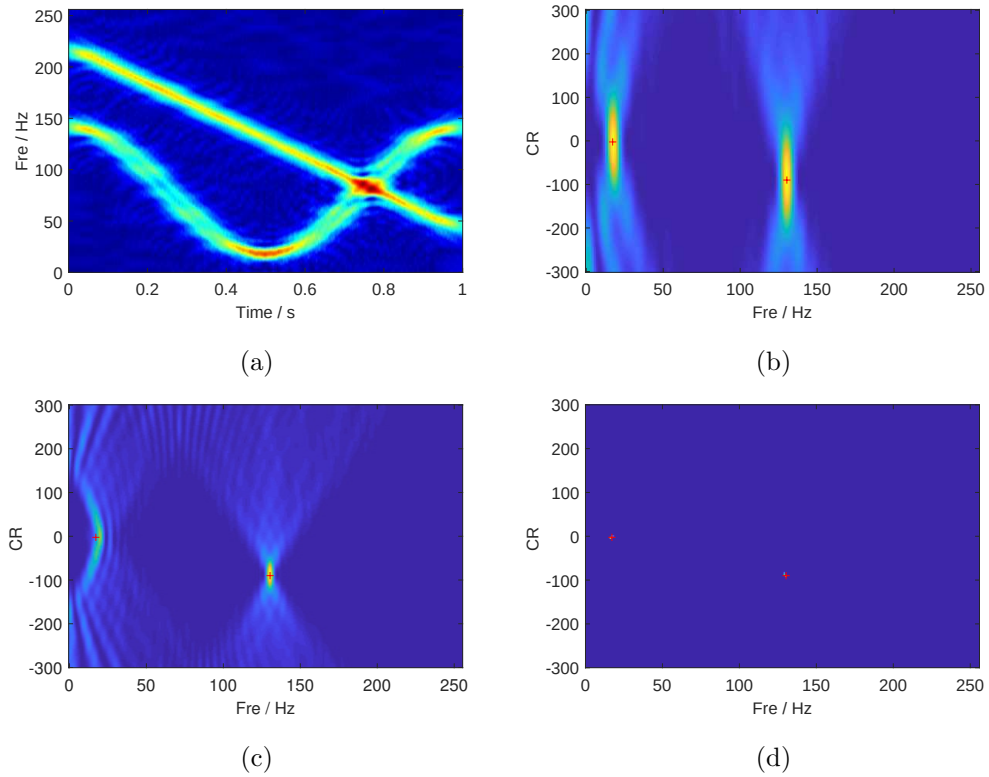

Figure 1: The STFT and the CT slices ($t = 0.5$ s) for the test signal. (a) The STFT, (b) the CT slice when window length is taken as 67 points, (c) the CT slice when the window length is taken as 127 points, (d) the FCRM result with 67 window length.

As the Gaussian window function $g(t) = \sigma^{-\frac{1}{2}} e^{-\frac{t^2}{2\sigma^2}}$ is employed, the CT result of $f(t)$ under the hypothesis (4) is simple gaussian integral as follows:

$$\begin{aligned} C_f^g(t,\omega,\beta) &= \int_{-\infty}^{+\infty} f(\mu) g(\mu - t) e^{-\frac{j\beta(\mu-t)^2}{2}} e^{-j\omega(\mu-t)} d\mu \\ &= f(t)\sqrt{\sigma}\sqrt{\frac{2\pi}{1 + j\sigma^2(\beta - \phi''(t))}} \exp\left(- \frac{\sigma^2(\omega - \phi'(t))^2}{2(1 + j\sigma^2(\beta - \phi''(t)))}\right). \end{aligned} \tag{5}$$

From (5), we can obtain that

$$\frac{1 + \sigma^4(\beta - \phi''(t))^2}{\sigma^2} \Re\left\{ \frac{\frac{\partial}{\partial\omega} C_f^g(t,\omega,\beta)}{C_f^g(t,\omega,\beta)} \right\} + \omega = \phi'(t), \tag{6}$$

$$\Im\left\{ \frac{C_f^g(t,\omega,\beta)^2}{\frac{\partial^2}{\partial\omega^2} C_f^g(t,\omega,\beta) \times C_f^g(t,\omega,\beta) - \frac{\partial}{\partial\omega} C_f^g(t,\omega,\beta)^2} \right\} + \beta = \phi''(t), \tag{7}$$

where $|\ C_f^g(t,\omega,\beta)\ | > \gamma$, $|\ \frac{\partial^2}{\partial\omega^2} C_f^g(t,\omega,\beta) \times C_f^g(t,\omega,\beta) - \frac{\partial}{\partial\omega} C_f^g(t,\omega,\beta)^2\ | > \gamma$, the parameter $\gamma > 0$ is a hard threshold, and $\Re\{\cdot\}$ ($\Im\{\cdot\}$) denotes the real (imaginary) part of complex number.

Let

$$\hat{\beta}(t,\omega,\beta) := \Im\left\{ \frac{C_f^g(t,\omega,\beta)^2}{\frac{\partial^2}{\partial\omega^2} C_f^g(t,\omega,\beta) \times C_f^g(t,\omega,\beta) - \frac{\partial}{\partial\omega} C_f^g(t,\omega,\beta)^2} \right\} + \beta, \tag{8}$$

then we can obtain the following expression according to equation (6)

$$\hat{\omega}(t,\omega,\beta) := \frac{1}{\sigma^2}\Re\left\{\frac{\frac{\partial}{\partial\omega}C_f^g(t,\omega,\beta)\mid_{\beta=\hat{\beta}}}{C_f^g(t,\omega,\hat{\beta})}\right\} + \omega = \phi'(t). \tag{9}$$

From expressions (8-9), a novel time-frequency-chirprate representation called the frequency-chirprate reassignment method (FCRM) is proposed as

$$Fc(t,\eta,\zeta) = \int_{-\infty}^{+\infty}\int_{-\infty}^{+\infty} \mid C_f^g(t,\omega,\beta)\mid^2 \delta(\eta-\hat{\omega})\delta(\zeta-\hat{\beta})d\omega d\beta, \tag{10}$$

where $\delta(\cdot)$ is the Dirac delta function. We call this transform as the frequency-chirprate reassignment because the reassignment is performed on the frequency-CR plane and it relocates the frequency-CR points from (ω,β) to $(\hat{\omega},\hat{\beta})$. The point $(\hat{\omega},\hat{\beta})$, an approximation of $(\phi'(t),\phi''(t))$, is called the reassignment center since the modulus of CT at that point achieves the maximum. Different from the standard RM [13], FCRM can be seen as a scaled reassignment since the scaling factor $\frac{1}{\sigma^2}$ is employed in expression (9).

Fig. 2 illustrates the reassignment of the signal representation to the new frequency-CR coordinates according to Equation (10), and the reassignment result is presented in Fig. 1(d). Obviously, the resulting FCRM has two peaks at the correct frequency-CR centers. Compared with the results obtained by CT (i.e., Fig. 1(b,c)), the proposed FCRM effectively improves the readability, obtaining highly concentrated frequency-CR representation.

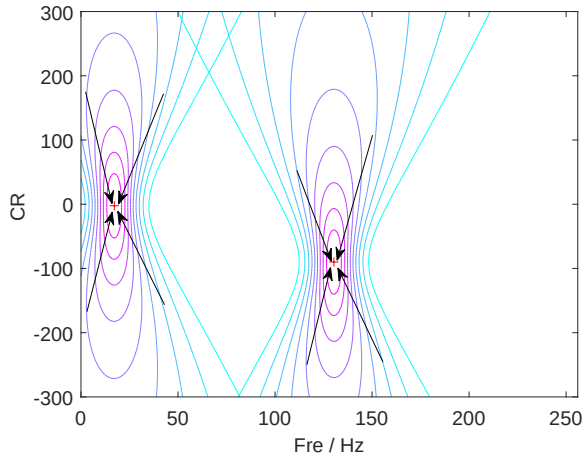

Figure 2: An illustration of the frequency-CR reassignment.

For more precise parameter estimation, $\frac{\partial}{\partial\omega}C_f^g(t,\omega,\beta)$ can be calculated by

$$\begin{aligned}\frac{\partial}{\partial\omega}C_f^g(t,\omega,\beta) &= \frac{\partial}{\partial\omega}\left(\int_{-\infty}^{+\infty} f(\mu)g(\mu-t)e^{-j\beta(\mu-t)^2/2}e^{-j\omega(\mu-t)}d\mu\right)\\ &= -jC_f^{tg}(t,\omega,\beta),\end{aligned} \tag{11}$$

where $C_f^{tg}(t,\omega,\beta)$ denotes the CT of $f(t)$ obtained by using the window function $tg(t)$. Similarly, for

$\frac{\partial^2}{\partial\omega^2}C_f^g(t,\omega,\beta)$, we also have

$$\frac{\partial^2}{\partial\omega^2}C_f^g(t,\omega,\beta) = -C_f^{t^2g}(t,\omega,\beta), \tag{12}$$

where $C_f^{t^2g}(t,\omega,\beta)$ denotes the CT of $f(t)$ under the window function $t^2g(t)$. Combing (11)-(12), the reassignment center can be computed by

$$\begin{cases} \hat{\beta}(t,\omega,\beta) = \Im\left\{\frac{C_f^g(t,\omega,\beta)^2}{C_f^{tg}(t,\omega,\beta)^2 - C_f^{t^2g}(t,\omega,\beta)C_f^g(t,\omega,\beta)}\right\} + \beta, \\ \hat{\omega}(t,\omega,\beta) = \Im\left\{\frac{C_f^{tg}(t,\omega,\hat{\beta})}{C_f^g(t,\omega,\hat{\beta})}\right\} + \omega. \end{cases} \tag{13}$$

Therefore, the computational cost of FCRM mainly comes from the CT calculations with different windows, and which can be efficiently implemented by FFT.

4. Three-dimensional ridge detection algorithm

In this section, we introduce a classical ridge detection algorithm to obtain the IF and CR estimates from three-dimensional signal representation.

FCRM reassigns the signal energy, which makes the representation achieve a maximum energy along the curve $(\phi'(t), \phi''(t))$, $t \in R$. Similar to the ridge definition given in the TF domain [41,55], we also call the maximum energy curve in the TFCR representation as the ridge. Due to the smoothness of the ridge curve, we can compute them by maximizing the cost function as

$$E(r(t),c(t)) = \int_{-\infty}^{+\infty} Fc(t,r(t),c(t))dt - \lambda_1\int_{-\infty}^{+\infty} r'(t)^2dt - \lambda_2\int_{-\infty}^{+\infty} c'(t)^2dt, \tag{14}$$

where λ_1 and λ_2 are two positive parameters tuning the level of regularization.

Consider the discrete multicomponent signal as

$$f(n) := \sum_{k=1}^{K} f_k(n\Delta t), \quad n = 1,2,\cdots,N, \tag{15}$$

where Δt is the sampling interval, Algorithm 1 offers algorithmic means to compute the ridges of the FCRM by optimizing the cost (14).

To improve the robustness of the detection procedure, several random initializations are required, leading to the detection of many different ridge sets $(r_k(t), c_k(t))$, and the one retained as the output corresponds to the one maximizing the cost (14). Moreover, the classical robust regression [56] can be applied to the obtained ridges to further improve the accuracy of the IF and CR estimation. It is worth noting that the introduced ridge detector can be directly applied to other three-dimensional representations instead of the FCRM in Algorithm 1.

5. Numerical validation

In this section, the proposed FCRM is tested on some numerical simulations. We employ the hard threshold method used in [20,26] to select parameter γ, and the Gaussian window is used in the FCRM.

Algorithm 1 Three-dimensional ridge detection algorithm

1: Input the TFCR representation $Fc(n,m,l)$, $1 \le n \le N$, $1 \le m \le M$, $1 \le l \le L$, the parameters λ_1, λ_2, and the allowable variations Δr and Δc;
2: Pick $q \in \{1, 2, \cdots, N\}$;
3: Define $(r(q), c(q)) = \arg\max_{m,l} Fc(q,m,l)$;
4: **for** $n = q+1, q+2, \cdots, N$ **do**
5: Define $I_{rc} = [\max(1, r(n-1) - \Delta r) \ \min(r(n-1) + \Delta r, M)] \times [\max(1, c(n-1) - \Delta c) \ \min(c(n-1) + \Delta c, L)]$;
6: Calculate $(r(n), c(n)) = \arg\max_{(m,l)\in I_{rc}} Fc(n,m,l) - \lambda_1 (m - r(n-1))^2 - \lambda_2 (l - c(n-1))^2$;
7: **end for**
8: **for** $n = q-1, q-2, \cdots, 1$ **do**
9: Define $I_{rc} = [\max(1, r(n+1) - \Delta r) \ \min(r(n+1) + \Delta r, M)] \times [\max(1, c(n+1) - \Delta c) \ \min(c(n+1) + \Delta c, L)]$;
10: Calculate $(r(n), c(n)) = \arg\max_{(m,l)\in I_{rc}} Fc(n,m,l) - \lambda_1 (m - r(n+1))^2 - \lambda_2 (l - c(n+1))^2$;
11: **end for**
12: Define $Fc(n,m,l) = 0$ for $(m,l) \in I_{rc}, n = 1, 2, \cdots, N$;
13: Repeat the steps (2-12) until all ridges are detected.

5.1. Overlapped multi-component signals detection

The first test is to consider the performance of the FCRM in detecting the two-components signal (3) with the SNR= 12 dB. Fig. 3 displays two frequency-CR plots of the CT and FCRM methods with an 67-length window, where the red notes are the true instantaneous information of the signal. Obviously, the FCRM successfully localizes the two modes and achieves a significant improvement on signal concentration compared with the CT. Although both two components of the signal (3) have almost the same IF at $t = 0.76$ s, the FCRM can separate them in the frequency-CR domain (see Fig. 3(d)). Furthermore, we apply Algorithm 1 ($\lambda_1 = 0.07$, $\lambda_2 = 0.03$) to the FCRM, and the detected results are displayed in Fig. 4. We can see from the results that the FCRM successfully characterizes the features of the overlapped multi-component signal, obtaining a good IFs estimation. It is difficult to separate this multi-component signal from the TF domain or time-CR domain due to the interference of different modes. It can be seen from Fig. 4(c) that a error exists in the CR estimation for FCRM. Nevertheless, the obtained CR information still plays a critical role in the TFCR representation because it contributes to a more accurate IF estimation for signals with cross-over frequencies.

In addition, Fig. 5(a,b) show the TF representations of the SST [20] and RM [13], and the estimated IFs by the TF ridge detection algorithm [55] are given in Fig. 5(c,d). Compared to the result of the FCRM as presented in Fig. 4(b), we can observe that SST and RM methods generate an inaccurate IFs estimation in the non-separable region, and easily leading to the mixture of different modes. Therefore, the TFCR representation has its clear advantages in processing multi-component non-stationary signals in spite of increasing the calculation than TF analysis methods.

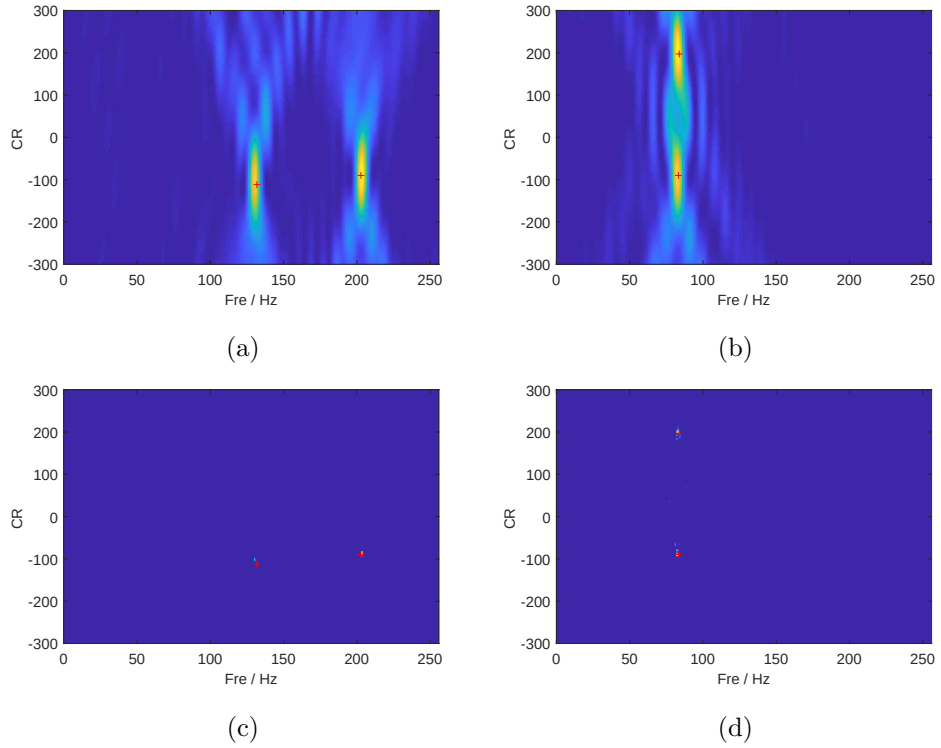

Figure 3: Frequency-CR plots by CT and FCRM at different times. (a) The CT result at $t = 0.1$ s, (b) the CT result at $t = 0.76$ s, (c) the FCRM result at $t = 0.1$ s, (d) the FCRM result at $t = 0.76$ s.

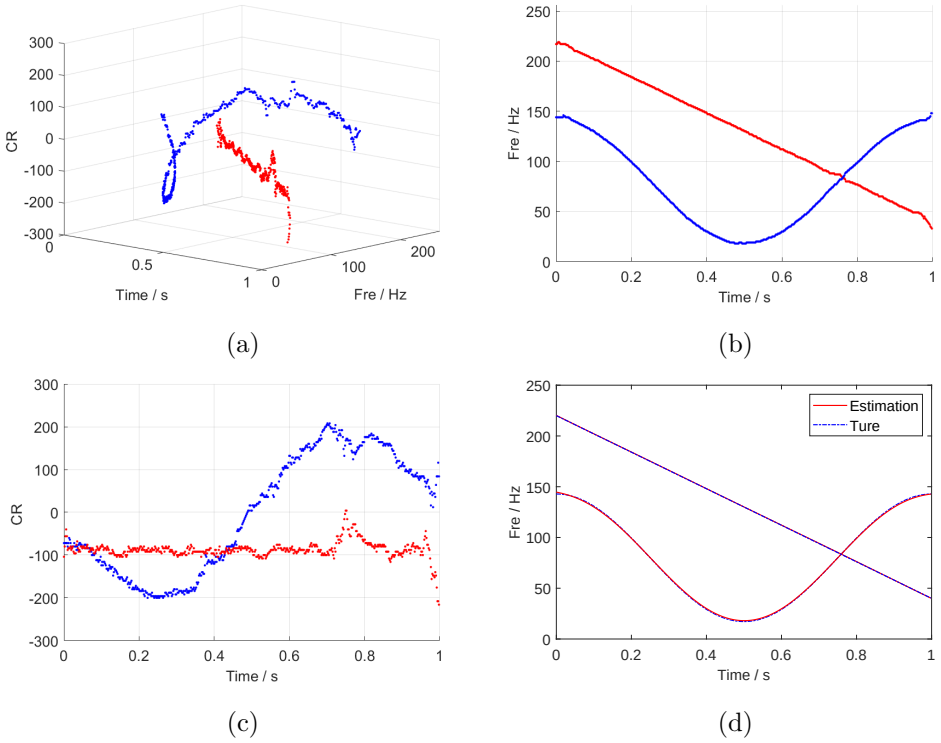

Figure 4: The detected result of FCRM. (a) Time-frequency-chirprate representation of FCRM, (b) TF plot of FCRM, (c) time-CR plot of FCRM, (d) the estimated IFs by FCRM.

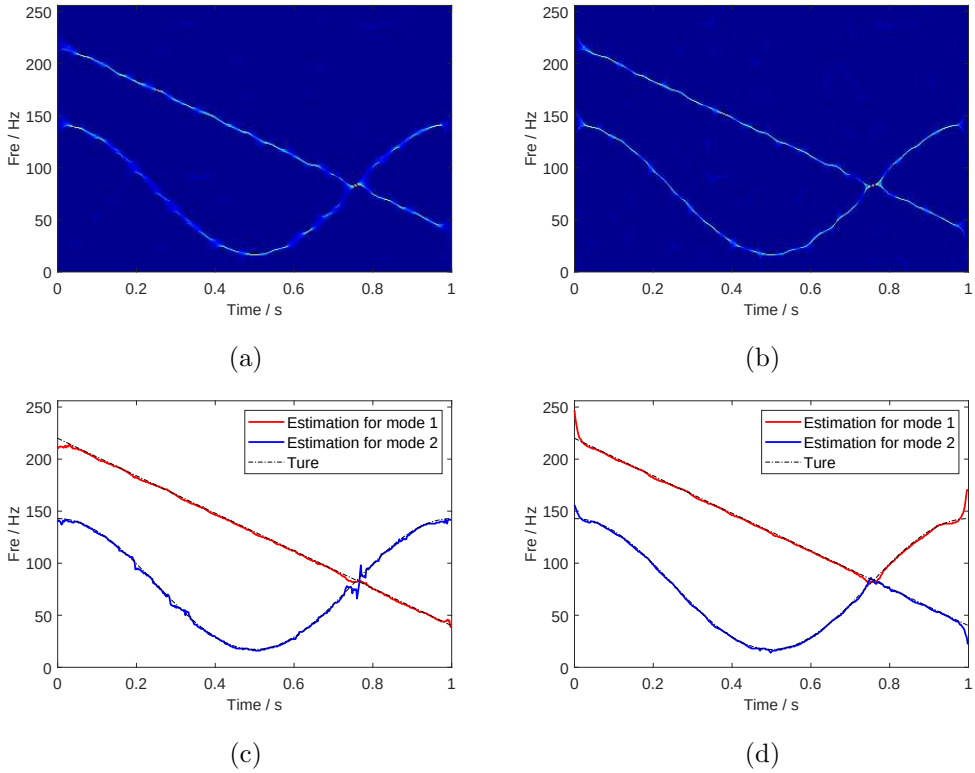

Figure 5: TF results of SST and RM. (a) SST result, (b) RM result, (c) the detected IF from SST, (d) the detected IF from RM.

Next, let us consider a three-components AM-FM signal with small CR values as

$$\begin{aligned} f(t) &= f_1(t) + f_2(t) + f_3(t) + n(t), \\ f_1(t) &= \cos(2\pi \times (0.35 + 85t - 8t^2)), \\ f_2(t) &= (1 + 0.1\cos(0.6\pi t))\cos(2\pi \times (20t + 12t^2)), \\ f_3(t) &= \cos(8\pi t + 120\sin(0.5\pi t)), \end{aligned} \tag{16}$$

where $n(t)$ is a Gaussian noise with the SNR= 8 dB. The sampling frequency is 256 Hz, and time duration is [0 4].

Fig. 6 provides two examples of the CT and FCRM for $t = 1.60$ s and $t = 2.34$ s. The results again prove the concentration ability of the FCRM. From Fig. 6(a,c), we also see that there are two modes overlapping in the frequency-CR plane for the CT method, while the FCRM shows a separated representation. We note one shortcoming of the FCRM is that it may yield error in locating the true CR, but that has little influence on the IF estimation. As presented in Fig. 7, the FCRM achieves a good IFs detection, which in turn brings a perfect result for CR estimation because of the derivative relation between the IF and the CR. In addition, Fig. 8 displays the TF results obtained by the SST and RM methods. It can be observed that, in the TF plane around the cross point, there are heavy cross-terms between two modes, and the TF methods cannot characterize the true IF trajectories. By comparison, the

proposed method generates a concentrated three-dimensional representation and has obvious advantages in addressing overlapped multi-component signals.

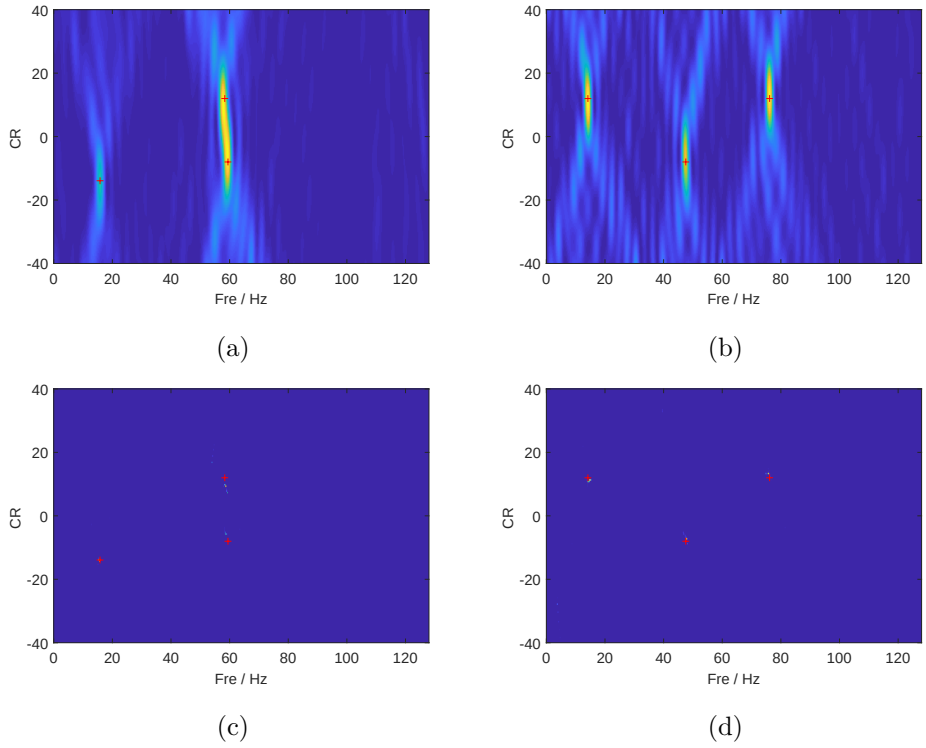

Figure 6: Frequency-CR plots by CT and FCRM at different times. (a) The CT result at $t = 1.60$ s, (b) the CT result at $t = 2.34$ s, (c) the FCRM result at $t = 1.60$ s, (d) the FCRM result at $t = 2.34$ s.

5.2. Performance in robustness to noise

In order to explore the performance of the FCRM method in noise tolerance, in this section we give the IF estimates of signal (3) under different noise levels. Similarly, the SST and RM methods are used for comparison. The detected result can be evaluated by the mean square error (MSE), which is calculated by

$$\mathrm{MSE} = \frac{1}{N} \parallel \widetilde{\mathrm{IF}} - \mathrm{IF} \parallel_2^2, \tag{17}$$

where N is the discrete length of the IF, $\| \cdot \|_2$ denotes l_2-norm, IF is the original clean IF, and $\widetilde{\mathrm{IF}}$ represents the estimated IF. The experiments are conducted by running 30 times and the average performance is recorded as the final result.

Fig. 9 displays the MSEs for the two IFs of the test signal with respect to different input SNRs. We note the IF estimation obtained by the FCRM is more accurate than that of the SST and RM for all noise levels. The average improvements for $f_1(t)$ and $f_2(t)$ are 2.1 and 1.3 in $\log 10$ scale than the standard RM. Therefore, the FCRM has a robust performance in component separation and IF estimation.

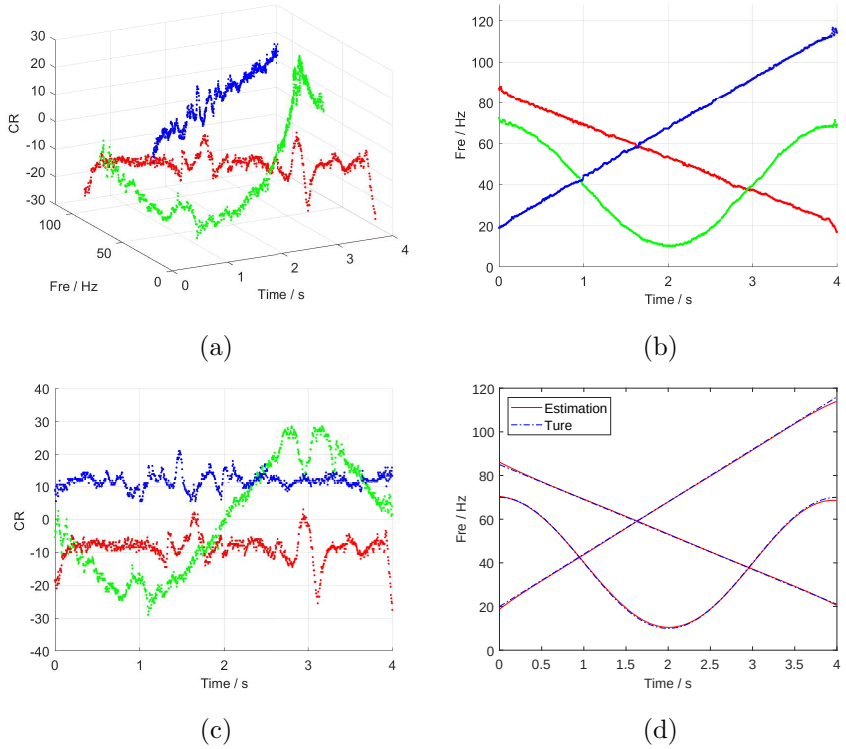

Figure 7: The detected result of FCRM. (a) Time-frequency-chirprate representation of FCRM, (b) TF plot of FCRM, (c) time-CR plot of FCRM, (d) the estimated IFs by FCRM.

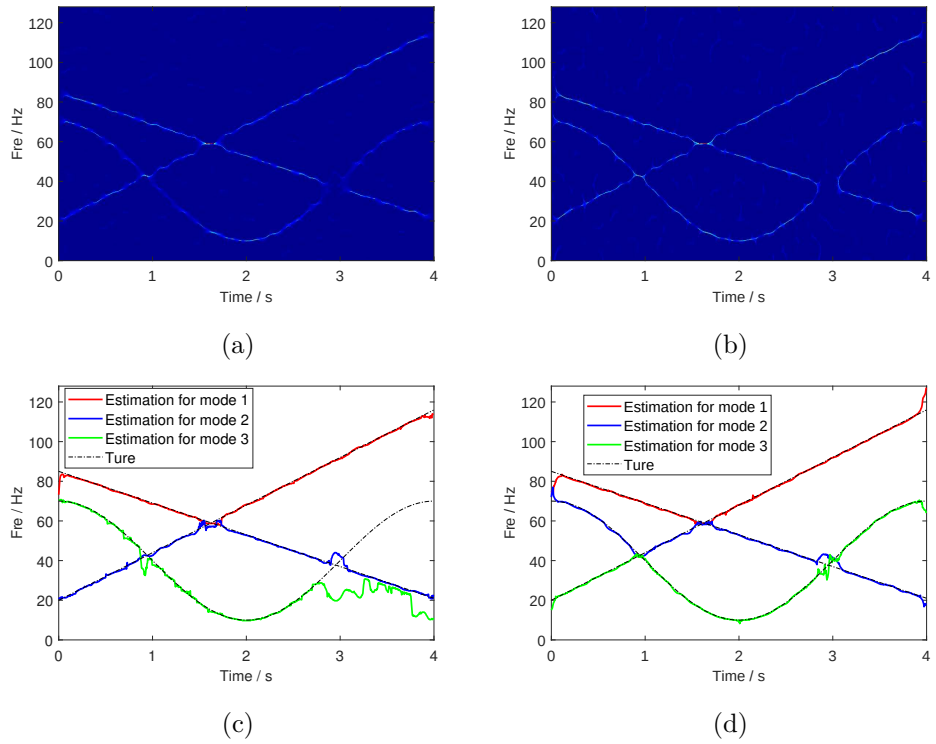

Figure 8: TF results of SST and RM. (a) SST result, (b) RM result, (c) the detected IF by SST, (d) the detected IF by RM.

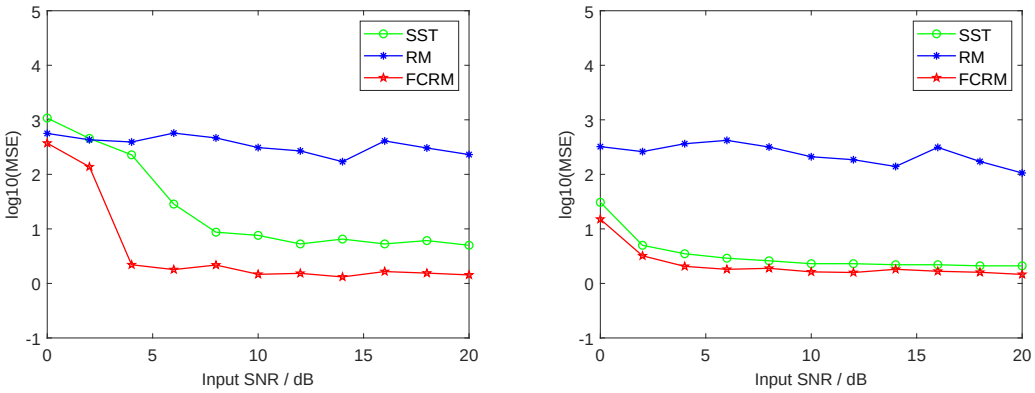

Figure 9: MSE of IF estimation versus SNR. (a) The MSEs of $f_1(t)$ by different methods, (b) the MSEs of $f_2(t)$ by different methods.

6. Conclusion

In this paper, a concentrated time-frequency-chirprate (TFCR) representation for multi-component non-stationary signals analysis has been proposed. The proposed FCRM relocates the frequency-CR points from their original locations to reassignment centers; it provides joint IF and CR estimation, which makes the TF crossed signals separated in the FCRM representation. To obtain robust IF and CR estimates form the FCRM, three-dimensional ridge detector is introduced. We finally apply the proposed method to analyze some simulation signals. The simulation results indicate that FCRM achieves a high-resolution TFCR representation, suitable for more accurate IF estimation in addressing overlapped multi-component signals. Future research will be devoted to the extension of the method to non-constant amplitude signals and to scalogram reassignment; more accurate CR estimation instead of Equation (8) and the application to real-life signals will be further investigated.

Acknowledgements

This work was partially supported by the Major Research Plan of the National Natural Science Foundation of China under grant no. 91730306 and the National Key R and D Program of the Ministry of Science and Technology of China under Grant no. 2018YFC0603501.

References

[1] N. Liu, J. Gao, B. Zhang, Q. Wang, X. Jiang, Self-adaptive generalized S-transform and its application in seismic time-frequency analysis, IEEE Trans. Geosci. Remote Sens. 57 (10) (2019) 7849-7859.

[2] S. Liu, T. Shan, Y.D. Zhang, Detection of weak astronomical signals with frequency-hopping interference suppression, Dig. Signal Process. 72 (2018) 1-8.

[3] X. Xia, Discrete chirp-Fourier transform and its application to chirp rate estimation, IEEE Trans. Signal Process. 48 (11) (2000) 3122-3133.

[4] C. Park, D. Looney, P. Kidmose, M. Ungstrup, D.P. Mandic, Time-frequency analysis of EEG asymmetry using bivariate empirical mode decomposition, IEEE Trans. Neural Syst. Rehabil. Eng. 19 (4) (2011) 366-373.

[5] S. Liu, Z. Zeng, Y.D. Zhang, T. Fan, T. Shan, R. Tao, Automatic human fall detection in fractional Fourier domain for assisted living, in Proc. 2016 IEEE International Conference on Acoustics, Speech and Signal Processing, Shanghai, China, 2016, pp. 799-803.

[6] Z. Feng, M. Liang, F. Chu, Recent advances in time-frequency analysis methods for machinery fault diagnosis: a review with application examples, Mech. Syst. Signal Process. 38 (1) (2013) 165-205.

[7] S. Wang, X. Chen, I.W. Selesnick, Y. Guo, C. Tong, X. Zhang, Matching synchrosqueezing transform: A useful tool for characterizing signals with fast varying instantaneous frequency and application to machine fault diagnosis, Mech. Syst. Signal Process. 100 (2018) 242-288.

[8] L. Cohen, Time-Frequency Analysis, Prentice-Hall, Englewood Cliffs, NJ, 1995.

[9] M.R. Portnoff, Time-frequency representation of digital signals and systems based on short-time Fourier analysis, IEEE Trans. Acoust. Speech Signal Process. 28 (1) (1980) 55-69.

[10] A. Grossmann, J. Morlet, Decomposition of hardy functions into square integrable wavelets of constant shape, SIAM J. Math. Anal. 15 (4) (1984) 723-736.

[11] T. Claasen, W. Mecklenbräuker, The Wigner distribution-a tool for time-frequency signal analysis-Part I: Continuous-time signals, Philips J. Res. 35 (1980) 217-250.

[12] K. Kodera, R. Gendrin, C. Villedary, Analysis of time-varying signals with small BT values, IEEE Trans. Acoust. Speech Signal Process. 26 (1978) 64-76.

[13] F. Auger, P. Flandrin, Improving the readability of time-frequency and time-scale representations by the reassignment method, IEEE Trans. Signal Process. 43 (5) (1995) 1068-1089.

[14] K. Fitz, L. Haken, On the use of time frequency reassignment in additive sound modeling, J. Audio Eng. Soc. 50 (11) (2002) 879-893.

[15] X. Wu, T. Liu, Spectral decomposition of seismic data with reassigned smoothed pseudo Wigner Ville distribution, J. Appl. Geophys. 68 (3) (2009) 386-393.

[16] J. Brynolfsson, M. Sandsten, Parameter estimation of oscillating Gaussian functions using the scaled reassigned spectrogram, Signal Process. 150 (2018) 20-32.

[17] F. Auger, P. Flandrin, Y. Lin, S. McLaughlin, S. Meignen, T. Oberlin, H.T. Wu, Time-frequency reassignment and synchrosqueezing: an overview, IEEE Signal Process. Mag. 30 (6) (2013) 32-41.

[18] V. Bruni, M. Tartaglione, D. Vitulano, A fast and robust spectrogram reassignment method, Mathematics 7 (4) (2019) 360.

[19] I. Daubechies, S. Maes, A nonlinear squeezing of the continuous wavelet transform based on auditory nerve models, in: A. Aldroubi, M. Unser (Eds.), Wavelets in Medicine and Biology, CRC Press, 1996, pp. 527-546.

[20] I. Daubechies, J.F. Lu, H.T. Wu, Synchrosqueezed wavelet transforms: an empirical mode decomposition-like tool, Appl. Computat. Harmon. Anal. 30 (2011) 243-261.

[21] G. Thakur, H.T. Wu, Synchrosqueezing-based recovery of instantaneous frequency from nonuniform samples, SIAM J. Math. Anal. 43 (5) (2012) 2078-2095.

[22] H. Yang, L. Ying, Synchrosqueezed curvelet transform for two dimensional mode decomposition, SIAM. J. Math. Anal. 46 (3) (2014) 2052-2083.

[23] H. Yang, L. Ying, Synchrosqueezed wave packet transform for 2D mode decomposition, SIAM J. Imaging Sci. 6 (2013) 1979-2009.

[24] H. Yang, Synchrosqueezed wave packet transforms and diffeomorphism based spectral analysis for 1D general mode decompositions, Appl. Computat. Harmon. Anal. 39 (1) (2015) 33-66.

[25] Z. Huang, J. Zhang, Z. Zou, Synchrosqueezing S-transform and its application in seismic spectral decomposition, IEEE Trans. Geosci. Remote Sens. 54 (2) (2016) 817-825.

[26] X. Zhu, Z. Zhang, Z. Li, J. Gao, X. Huang, G. Wen, Multiple squeezes from adaptive chirplet transform, Signal Process. 163 (2019) 26-40.

[27] G. Thakur, E. Brevdo, N.S. Fučkar, H.T. Wu, The Synchrosqueezing algorithm for time-varying spectral analysis: Robustness properties and new paleoclimate applications, Signal Process. 93 (2013) 1079-1094.

[28] I. Daubechies, Y. Wang, H.T. Wu, ConceFT: concentration of frequency and time via a multitapered synchrosqueezed transform, Philos. Trans. R. Soc. 374 (2065) (2016) 20150193.

[29] H. Yang, Statistical analysis of synchrosqueezed transforms, Appl. Computat. Harmon. Anal. 45 (3) (2018) 526-550.

[30] A. Ahrabian, D. Looney, L. Stanković, D.P. Mandic, Synchrosqueezing-based time-frequency analysis of multivariate data, Signal Process. 106 (2015) 331-341.

[31] L. Stanković, D. Mandić, M. Daković, M. Brajović, Time-frequency decomposition of multivariate multicomponent signals, Signal Process. 142 (2018) 468-479.

[32] C. Li, M. Liang, A generalized synchrosqueezing transform for enhancing signal time-frequency representation, Signal Process. 92 (2012) 2264-2274.

[33] T. Oberlin, S. Meignen, V. Perrier, Second-order synchrosqueezing transform or invertible reassignment? Towards ideal time-frequency representations, IEEE Trans. Signal Process. 63 (2015) 1335-1344.

[34] S. Meignen, T. Oberlin, D.H. Pham, Synchrosqueezing transforms: From low- to high-frequency modulations and perspectives, C. R. Phys. 20 (2019) 449-460.

[35] E.J. Candes, P.R. Charlton, H. Helgason, Detecting highly oscillatory signals by chirplet path pursuit, Appl. Comput. Harmon. Anal. 24 (1) (2008) 14-40.

[36] S. Wang, X. Chen, G. Cai, B. Chen, X. Li, Z. He, Matching demodulation transform and synchrosqueezing in time-frequency analysis, IEEE Trans. Signal Process. 62 (1) (2014) 69-84.

[37] D.H. Pham, S. Meignen, High-order synchrosqueezing transform for multicomponent signals analysis-with an application to gravitational-wave signal, IEEE Trans. Signal Process. 65 (12) (2017) 3168-3178.

[38] G. Yu, Z. Wang, P. Zhao, Multi-synchrosqueezing Transform, IEEE Trans. Ind. Electron. 66 (7) (2019) 5441-5455.

[39] D. He, H. Cao, S. Wang, X. Chen, Time-reassigned synchrosqueezing transform: The algorithm and its applications in mechanical signal processing, Mech. Syst. Signal Process. 117 (2019) 255-279.

[40] G. Yu, M. Yu, C. Xu, Synchroextracting transform, IEEE Trans. Ind. Electron. 64 (10) (2017) 8042-8054.

[41] X. Zhu, Z. Zhang, J. Gao, B. Li, Z. Li, X. Huang, G. Wen, Synchroextracting chirplet transform for accurate IF estimate and perfect signal reconstruction, Dig. Signal Process. 93 (2019) 172-186.

[42] Z. Li, J. Gao, Z. Wang, A time-synchroextracting transform for the time-frequency analysis of seismic data, IEEE Geosci. Remote Sens. Lett., 2019, doi: 10.1109/LGRS.2019.2931138.

[43] V. Bruni, M. Tartaglione, D. Vitulano, On the time-frequency reassignment of interfering modes in multicomponent fm signals, in: Proc. 26th European Signal Processing Conference (EUSIPCO), Rome, 2018, pp.722-726.

[44] V. Bruni, M. Tartaglione, D. Vitulano, An iterative approach for spectrogram reassignment of frequency modulated multicomponent signals, Math. Comput. Simulat., 2019, doi: https://doi.org/10.1016/j.matcom.2019.11.006.

[45] S. Chen, X. Dong, G. Xing, Z. Peng, W. Zhang, G. Meng, Separation of overlapped non-stationary signals by ridge path regrouping and intrinsic chirp component decomposition, IEEE Sensors J. 17 (18) (2017) 5994-6005.

[46] P. Li, Q. Zhang, IF estimation of overlapped multicomponent signals based on viterbi algorithm, Circuits Syst. Signal Process., 2019, doi: 10.1007/s00034-019-01314-8.

[47] B. Porat, B. Friedlander, Asymptotic statistical analysis of the high order ambiguity function for parameter estimation of polynomial-phase signals, IEEE Trans. Inform. Theor. 42 (3) (1996) 995-1001.

[48] P. O'Shea, A new technique for instantaneous frequency rate estimation, IEEE Signal Process. Lett. 9 (8) (2002) 251-252.

[49] I. Djurovic, M. Simeunovic, P. Wang, Cubic phase function: A simple solution to polynomial phase signal analysis, Signal Process. 135 (2017) 48-66.

[50] S. Mann, S. Haykin, The chirplet transform: physical considerations, IEEE Trans. Signal Process. 43 (11) (1995) 2745-2761.

[51] W. Zhang, Y. Fu, Y. Li, Sparse time-frequency-frequency-rate representation for multicomponent nonstationary signal analysis, in: Proc. 26th European Signal Processing Conference (EUSIPCO), Rome, 2018, pp.717-721.

[52] G. Yu, Y. Zhou, General linear chirplet transform, Mech. Syst. Signal Process. 70-71 (2016) 958-973.

[53] M. Aoi, K. Lepage, Y. Lim, U.T. Eden, T.J. Gardner, An approach to time-frequency analysis with ridges of the continuous chirplet transform, IEEE Trans. Signal Process. 63 (3) (2015) 699-710.

[54] X. Zhu, Z. Zhang, H. Zhang, J. Gao, B. Li, Generalized ridge reconstruction approaches toward more accurate signal estimate, Circuits Syst. Signal Process., 2019, doi: https://doi.org/10.1007/s00034-019-01278-9.

[55] S. Meignen, D.H. Pham, S. McLaughlin, On demodulation, ridge detection and synchrosqueezing for multicomponent signals, IEEE Trans. Signal Process. 65 (8) (2017) 2093-2103.

[56] P.J. Rousseeuw, A.M. Leroy, Robust Regression and Outlier Detection, John Wiley & Sons, 1987.